Analysis of WFPC-2 Core Samples for MMOD Discrimination

P. Anz-Meador [1], L. Le [1], M. Ward [1], K. Thomas-Keprta [2], and D.K. Ross [3]

[1]Jacobs, NASA Johnson Space Center, Mail Code XI5-9E, 2101 NASA Parkway, Houston, TX 77058, USA,
phillip.d.anz-meador@nasa.gov
[2]Barrios Technology Inc – Jacobs JETS Contract, NASA Johnson Space Center, Mail Code XI5-9E,
2101 NASA Parkway, Houston, TX 77058, USA
[3]University of Texas at El Paso – Jacobs JETS Contract, NASA Johnson Space Center, Mail Code XI5-9E,
2101 NASA Parkway, Houston, TX 77058, USA

ABSTRACT

An examination of the Hubble Space Telescope Wide Field Planetary Camera 2 (WFPC-2) radiator assembly was conducted at NASA Goddard Space Flight Center during the summer of 2009. Immediately apparent was the predominance of impact features, identified as simple or complex craters, resident only in the thermal paint layer; similar features were observed during a prior survey of the WFPC-1 radiator. Larger impact features displayed spallation zones, darkened areas, and other features not observed in impacts onto bare surfaces. Craters were extracted by coring the radiator in the NASA Johnson Space Center's Space Exposed Hardware cleanroom and were subsequently examined using scanning electron microscopy/energy dispersive X-ray spectroscopy to determine the likely origin, *e.g.*, micrometeoritic or orbital debris, of the impacting projectile. Recently, a selection of large cores was re-examined using a new technique developed to overcome some limitations of traditional crater imaging and analysis. This technique, motivated by thin section analysis, examines a polished, lateral surface area revealed by cross-sectioning the core sample. This paper reviews the technique, the classification rubric as extended by this technique, and results to date.

1   INTRODUCTION

The Hubble Space Telescope (HST) was designed for regular servicing during its operational lifetime by the Space Transportation System (STS; the Space Shuttle). STS servicing missions (SM) 1, 2, 3A, 3B, and 4 noted degradation of HST surfaces, as well as impact features evident on the HST bus and optical tube (thermal tape), multi-layer insulation (MLI) blankets, and the Wide Field Planetary Camera 2 (WFPC-2) radiators. The WFPC-2 instrument was returned to Earth in 2009 by the crew of STS-125's SM4. The radiator attached to WFPC-2 was surveyed optically for impact features by personnel from the Orbital Debris Program Office (ODPO) at NASA Johnson Space Center (JSC), Marshall Space Flight Center's Meteoroid Environment Office, and Goddard Space Flight Center (GSFC). A large number of craters produced by impactors were extracted from the radiator using an ODPO-developed, core sampling method. Several teams have since characterized and interpreted the crater residues on these cores using scanning electron microscopy (SEM) and energy dispersive X-ray spectroscopy (EDX) results [1, 2]. However, there are limitations such as analyzing residue present in larger (>100 μm) and deeper craters or the effects crater geometry can have on the collection of EDX spectra. To avoid the limitation of SEM/EDX techniques imposed by the sample geometry, a different approach has been developed for crater preparation: cross-sectioning prior to the analysis and determination of potential sources. Highlights, challenges, and results of previous analyses of WFPC-2 radiator core samples, including the cross-sectioning technique, are presented. In general, three overarching designations of impactors have been labelled based on their origin. These designations are: (1) Orbital Debris (OD); (2) Micrometeoroid (MM); and, (3) Undetermined (U). Detailed descriptions of these categories are given in [3]. While outside the scope of this paper, the observed cratering record, in concert with the HST's attitude history and laboratory-derived impact damage equations, is used to estimate the time-averaged, integrated debris flux. This estimate requires discrimination between the MM and OD components of the environment and this has been conducted to facilitate the validation of ODPO's latest OD engineering model (ORDEM).

2   BACKGROUND

The WFPC-2 camera was retrieved by SM 4/STS-125 in 2009 and returned after approximately 15.4 years exposure. The camera's radiator consisted of a 0.8 m x 2.2 m curved rectangular plate (1.76-m^2 surface area) conformal to the HST's outer surface and 60° in azimuthal extent. The 4.06 mm-thick aluminum (Al) 6061-T6 substrate was painted

with a 100-150 μm-thick layer of zinc orthotitanate (Zn_2TiO_4), YB-71 white thermal paint. The NASA ODPO mounted three expeditions to a NASA GSFC class 100 (ISO5) clean room in July-September 2009 to characterize the surface of the WFPC-2's radiator; 677 impact features, to a limiting feature size of approximately 300 μm, were observed and documented during these inspections.

In November 2009, the WFPC-2 was shipped and displayed at the Smithsonian National Air and Space Museum, the NASA Jet Propulsion Laboratory and the Denver Museum of Nature and Science. During these displays (Fig. 1), WFPC-2 was in a clear container that was neither purged nor airtight. After returning to storage in November 2010, the radiator was de-integrated from the camera assembly in September 2011 in GSFC's warehouse. Bagged in electrostatic dissipative sheets, the radiator was shipped to NASA JSC's Space Exposed Hardware (SEH) class 1000 (ISO4) clean room in December 2011 for coring and detailed inspection of MMOD impact features. Collecting core samples from the thick surface using a core drill offered the greatest probability of success within two major constraints: 1) not contaminating the sample during collection; and, 2) not compromising the integrity of the clean room in which sampling would be conducted (Fig. 2).
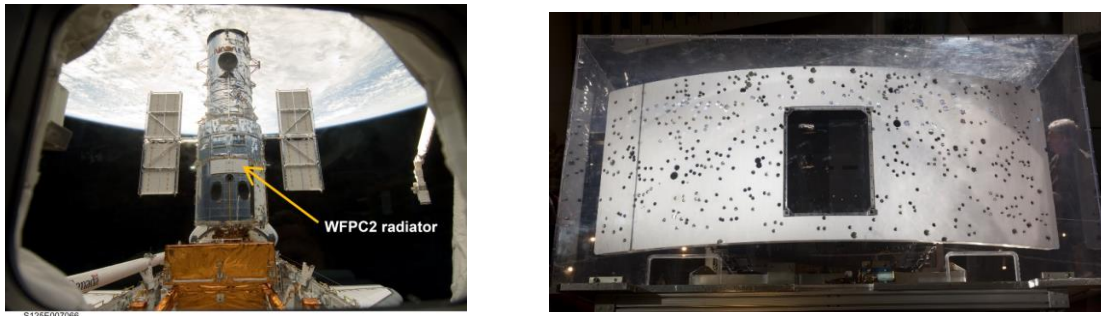

Fig. 1. *Left*: A view of the HST after it was captured and docked to the STS-125 Atlantis cargo bay, with the WFPC-2 radiator identified. *Right*: WFPC-2 radiator in display case.

A joint study between NASA and the European Space Agency (ESA) began in 2012, and the core sampling technique was developed to extract impact features on the radiator. Out of 480 large and small cores extracted, half went to ESA, to be curated at the United Kingdom's Natural History Museum and the University of Surrey's Ion Beam Centre, with the remaining cores to be investigated using the NASA Astromaterials Research and Exploration Science Directorate lab facility at NASA JSC. These impact features have all been examined using SEM and Particle Induced X-Ray Emissions (PIXE). Reports from ESA [4, 5, 6, 1, 7] and NASA JSC [8, 3] describe the findings. All core samples are maintained in a state to allow future analyses on the cores, should superior techniques be developed and implemented for the analysis of returned surfaces.
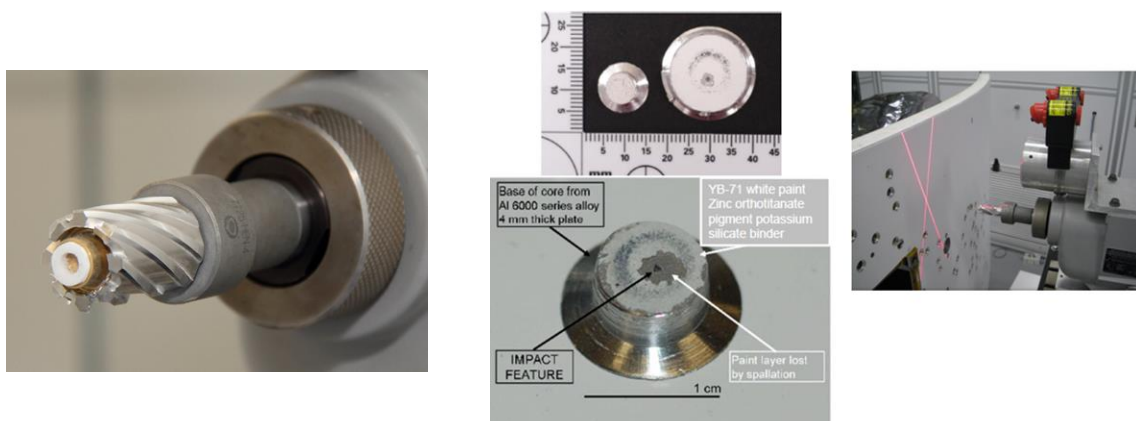

Fig. 2. *Left*: the encapsulating clean room coring tool developed by ODPO. *Center top*: ODPO small and large core exemplars. *Center bottom*: The core is composed of an Al 6061, 4 mm-thick substrate with its upper surface painted with YB-71 white space-rated thermal paint. The paint consists of Zn_2TiO_4 white pigment with a potassium-silicate PS7 binder. *Right*: coring device with laser alignment and positioning aid.

The method used in the current analysis was predicated upon prior sampling campaigns to characterize surfaces returned from space (*i.e.*, the Long Duration Exposure Facility [LDEF]). In these campaigns, samples or cores were cut from select surfaces and analyzed, using standard SEM-EDX techniques, to assess the elemental composition of the impactor. EDX specifically has shown to be an effective method to locate impact residues [6]. In the absence of this chemical mapping, the search for impactor residues can present a challenging search and identification problem though observation of impact melt can guide a search. Particularly for the larger impact features, the area that needs to be searched is very large relative to the area and volume sampled by electron-beam excitation in spot mode. The WFPC-2 radiator presents unique challenges due to its geometry (a rectangular section from a right circular cylinder's lateral surface), thickness, coating, and the size and extent of many impact features. This paper presents a new technique: looking at a polished flat surface (which eliminates angular issues and makes the seam/coating layer cross section visible), and cutting along the long axis and through the deepest part of a crater (using predetermined cut plans). Craters at JSC are first characterized with a preliminary examination using field emission SEM (FESEM) in conjunction with EDX, followed by embedding the crater in epoxy and subsequently slicing the crater to produce a section. The area of analysis is restricted to one section through the crater. Despite this potential limitation (while noting that a sample may be re-polished to reveal a new surface), the analysis scheme provides a better approach to determining impactor type by removing certain physical and instrumental constraints.

3   CLASSIFICATION

A priori, the origin of the impactor for any given crater is assumed micrometeoritic. This may then undergo reclassification to orbital debris, using a hierarchical binary decision framework, during subsequent investigation based on elemental analysis of particulates embedded within crater and/or the crater rim. The discriminating characteristic of orbital debris is the enrichment of specific elements and/or patterns in the abundance of particular elements, which are: (1) rarely, if ever, observed in chondritic meteorites; and (2) are common materials in spacecraft structures or components. If such particulates are identified within a given crater then it is classified as resulting from orbital debris. Furthermore, such observations take precedence over those of other particulates, within the same crater, which might otherwise be construed as meteoritic. That is, the decision as to a meteoritic or orbital debris origin for a crater is based on either the identification, or lack thereof, of spacecraft-associated materials.

Challenges in the identification of impactors in these hypervelocity impact features are posed by the chemical complexity of the impacted surface. The paint overlay includes elements that are common in impacts identified from work on STS window impactors. The paint is composed of Zn_2TiO_4 as the pigment, mixed with potassium silicate (PS7; K_2SiO_4) as a binder. Zn and Ti are common pigment constituents in space-flown hardware, and many impacts on space shuttle windows were attributed to impacts by Zn- and/or Ti-bearing paint fragments. Clearly, such impacts on the WFPC-2, painted radiator surface would be essentially impossible to distinguish from Zn and Ti already present. The Al alloy that underlies the painted surface is also complex. It is dominated by Al, but also includes abundant inclusions of metal alloys containing iron (Fe), chromium (Cr), manganese (Mn), copper (Cu), and silicon (Si). Other abundant inclusions are magnesium (Mg) Si-oxide. The presence of Fe-bearing inclusions in the alloy renders identifications of Fe-rich impactors problematic, and the presence of Mg and Si in the Al-alloy substrate renders the identification of MM impactors uncertain.

The rubric defined for impactor classification has three categories: MM, OD, and U. In the case of MM, constituents that are the best indicator include Mg, Fe, sulphur (S), nickel (Ni) and calcium (Ca). Magnesium rich silicates, Fe-Ni metal, Fe-Ni sulfides, Ca-bearing silicates, and Mg-Cr-rich oxides are further indicators of MM. The "U" category indicates that either nothing can be found or insufficient analysis was conducted.

4   PRIOR ANALYSES AND MOTIVATION FOR FURTHER SURVEY

In the joint NASA/ESA characterization process, cored samples were examined using two SEM instruments fitted with EDX detectors. If no unambiguous chemical compositions were revealed, an additional proton beam for PIXE was used. EDX spectra were collected for 200 seconds, 20kV accelerating voltage, and 3nA electron beam current. When X-ray peaks exceeded background X-ray by a factor of three, an element was "detected." Depth and profiles using backscattered electron imagery and X-ray element maps were made of impact features. The analysis team used Sections 3's rubric and decision trees to classify impactor origin. Presence of the elements dissolved in impact-melted paint indicates that these elements were present when the impact occurred, and were most plausibly added by the impacting particle. Approximately 79% of impact features examined at JSC yielded evidence for MM impactors. Less than 1% yielded evidence indicating orbital debris impactors, and the remaining 20% have been classed as undetermined, because no clear evidence could be located, which would permit distinguishing the type of impactor.

These results are consistent with conclusions reached by colleagues at the Natural History Museum of London and the Ion Beam Analysis Group in Surrey, England, who have investigated approximately half of the WFPC-2 cores at their facilities. These outcomes are illustrated in Table 1, specifically the "2014 Assessment" column, for a selection of WFPC-2 large impact features curated at NASA JSC. This categorization is, however, inconsistent with the STS window experience, as well as the expectation based on the NASA ORDEM 2000 model, which incorporated LDEF and HST solar panel impact feature data for build and validation, as constrained by the HST attitude history (approximately random orientation over the exposure) and the relative independence of the MM flux with altitude. For identified residues, the ratio of OD: MM is approximately 55%:45%. Of the OD contribution, 79% of the identified OD residues composed of paint and Al alloys could be impossible to identify uniquely on the complex WFPC-2 surface. Note that this does not alter the relative percentages of MM: OD: U, but rather would establish a category of undetermined residues, which are nonetheless OD. A common hypothesis regarding the unknown category is that the probability of sampling crater residues decreases as the relative velocity increases; however, this is applicable to both MM, OD [9], and represents a sampling bias based on relative velocity but not necessarily flux.

After considering this and other hypotheses regarding the nature of impactors resident in the undetermined category, there appears, at this time, to be no compelling argument against applying the frequentist statistical concept of treating the identified residues (588 impact features) as a sample approximating the relative proportions of MM and OD in the data set of 1986 window impact features. Comparing ORDEM 2000 model results with the Grün, *et al*. MM model [10] flux, ISS altitudes (approximating the STS operational environment) are approximately equivalent in MM: OD ratio. This is consistent with the STS window results for identified constituents, and extended to all impact features. However, at HST altitudes, OD was expected to predominate over MM by a factor of 2.25, the ratio of OD at HST to ISS altitudes, at 10 µm and larger sizes. This apparent discrepancy, with respect to analytical outcomes and given the complexity in both the mechanics of probing a crater and interpreting the findings therein, motivated a campaign to characterize residues with greater care on a sample-by-sample basis. These outcomes are presented in Table 1 as the "2017 Assessment" column for samples common to the two campaigns. As tabulated, 7 of 12 differed in assessment outcome, with 4 of 7 identities changing from MM to OD.

Table 1. Analytical outcomes for WFPC-2 large cores (note that letters "I" and "O" were not used to identify samples).

JSC core #	JSC Sample Letter	Lips/Center Diameter [µm]	Total Depth [µm]	2014 Assessment	2017 Assessment
471	A	1282.94	689.4	MM	OD
463	B	890.66	535.2	MM	OD
460	C	595.09	152.8	MM	UND
462	D	591.97	235.4	MM	OD
461	E	552.34	230.5	MM	UND
478	F	552.89	266.3	OD	OD
465	G	540.51	201.6	UND	MM
476	H	521.97	194.6	MM	MM
469	J	510.22	41.9	MM	MM
475	K	503.39	160.7	MM	MM
468	L	488.76	374.1	MM	OD
421	M	391.54	165.6	MM	MM

The analytical limitations of analyzing residue present in concave surface depressions, particularly in large (*e.g*., > 100 µm diameter) and deep craters using SEM/EDX have been discussed elsewhere in detail [11]. Specific to these discussions are the effects that crater geometry can have on the collection of EDX spectra. Because EDX detectors cannot be sighted normal to a sample surface, as this would be coincidental with the electron beam column, they necessarily are positioned at an acute angle above the sample surface (known as the take-off-angle for the detector). Thus, in craters with a high depth-to-diameter ratio, the line-of-sight can become partially or completely obscured between the EDX detector and the electron beam incident on the surface. This severely complicates analyses of materials at or near the crater bottom due to screening by the crater rim, which can lead to disproportionate increases in heavy element abundances due to the preferential absorption of low-energy X-rays.

5 NEW ANALYSIS PROCEDURES AND RESULTS

An internal, joint working group consisting of ODPO, the JSC Hypervelocity Impact Technology [HVIT] group, and the JSC Basic and Applied Research Department suggested that constraints imposed by these geometrical effects could be resolved by thin sectioning the core samples. The working group also recommended sectioning the cores into two semicircles along a "line of interest" and examining the residues present in the crater at the interface of the substrate and crater feature. The line of interest is defined by examining the crater at high magnification using a Keyence VHX-5000 digital microscope and identifying the plane intersecting the crater's longest dimension and the deepest portion of the crater. Such a section is illustrated in Fig. 3.
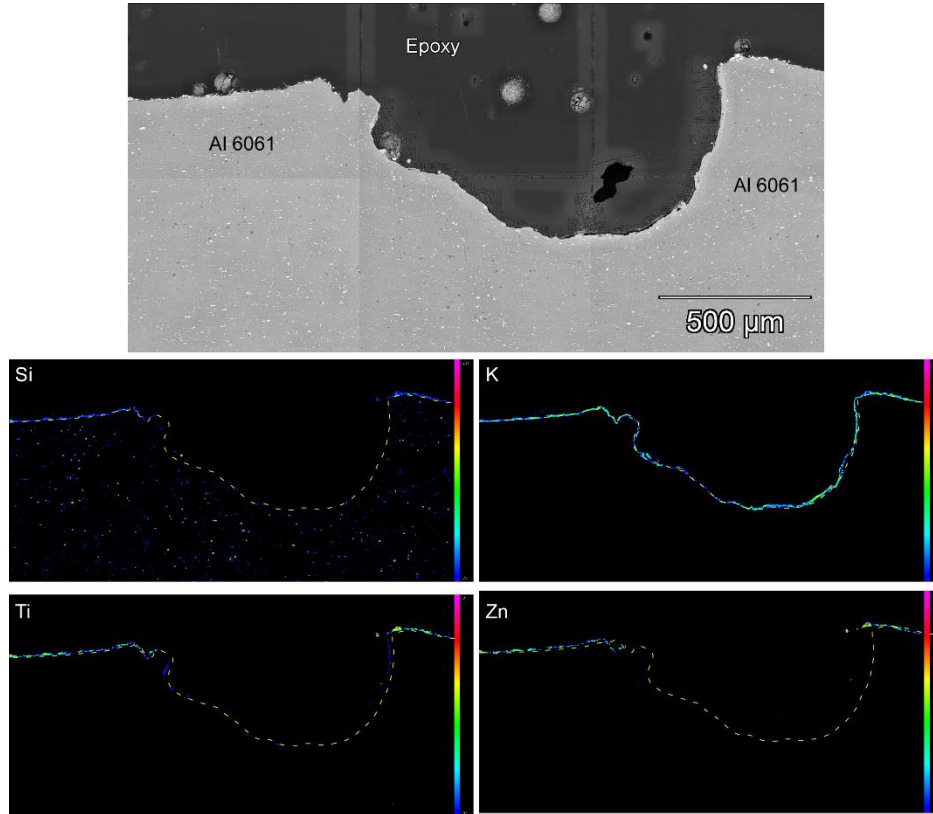

Fig. 3. *Upper*: FESEM/LABE image mosaic of the lateral surface of the cut core from crater A, core 471. *Lower*: Element X-ray mosaic maps for Si, potassium (K), Ti and Zn. Regions enriched in Si and K are binder and regions enriched in Ti and Zn are composed of paint. Potassium-rich regions not associated with Si are interpreted as potassium hydrogen carbonate. Yellow dash lines indicate the location of the edge of the Al 6061 matrix.

6 SAMPLES

Twenty-one carbon coated radiator cores, including Table 1's samples A-M, first were characterized using FESEM/EDX. Following preliminary evaluation, craters were embedded in a two-part (resin and hardener) transparent epoxy produced by Buehler. Based on Nikon SMZ800 optical microscope images of the crater surface, the ODPO line of interest was transcribed to a cross-sectioning line defined by position and orientation of the core. Using a South Bay Technology saw, craters were then sectioned along this line. After cutting, the surface of each exposed crater was placed back in the epoxy, followed by subsequent polishing using diamond oil-based suspension (1 μm; Buehler), then by polishing with Al-oxide (0.3 μm; Buehler). Finally, the section was cleaned thoroughly in an ultra-sonic bath using laboratory-grade ethyl alcohol. The polished section was air-dried and subsequently coated with a layer of sputtered carbon ~15 nm in thickness. The cutting and polishing process has been examined carefully, with the conclusion that no contamination occurs during these processes. The sample was characterized using a JEOL 7600 FESEM equiped with a light element Thermo Scientific EDX Silicon Drift Detector (SDD). Each crater was imaged using a low-angle, backscatter electron (LABE) detector and a composite mosaic image was produced. Higher magnification scanning electron/LABE views of regions of interest (ROIs) were collected for

90 seconds. The entire craters were also mapped using EDX for elements carbon (C), oxygen (O), sodium (Na), Mg, Al, Si, phosphorous (P), S, chlorine (Cl), K, Ca, Ti, Fe, Ni, Cu, and Zn and individual EDX spectra of ROIs were collected for times ranging from 30 – 200 seconds. Depending on count rates, analysis spot size ranged from ~ 0.5 μm -10 μm. Typically, EDX conditions of 15 kV and ~900 pA were used for analysis. In select cases, accelerating voltages ranging from 20-30 kV were used depending on the element of interest. In one case, Raman spectroscopy was used to characterize C-rich matter in a crater. Raman spectroscopy was used as a secondary verification tool to confirm identification of C-rich matter, and as a probe of the structural organization state of identified carbonaceous phases. While interpretation of Raman spectra can be difficult where multiple carbonaceous phases coexist in a single sample, it is nevertheless, a valuable tool in determining the nature of carbon when used in conjunction with other techniques. We used a WiTech Alpha300 μ-Raman spectrometer operating at a probe spatial resolution of ~ 1 μm and equipped with a helium-neon laser operating at a wavelength of 633 nm, coupled to an Olympus BX 41 optical microscope. The sample was scanned from 300–3000/3500 cm^{-1}. In Raman, pure monocrystalline graphite is identified by the presence of a single peak, designated as 'G' (graphite), with a Raman shift of ~ 1580–1600 cm^{-1}. In contrast, matter composed of polycrystalline graphite, amorphous C, or mixtures thereof, show an additional peak designated as 'D' (disorder), with a Raman shift of ~ 1350 cm^{-1} [12, 13].

7   SUMMARY OF RESULTS

Samples A-M, P, Q, and V have been reclassified as OD or likely OD, based upon the sectioning technique described in this paper, while the remaining samples have been tentatively identified as OD. Most had pseudo-circular perimeters although some appeared elliptical and a few had irregular external shapes. The majority have simple crater morphologies with a single central depression. Identification of impact, melt-rich, lithologies was based on established morphological and textural criteria, such as smooth/melt regions containing vesicles draped over irregular surfaces [11]. In every case, the paint/binder layer was absent to some extent in the crater interior with residual paint present, either intermixed with the impactor or as a thin, vesiculated veneer. In some craters, the Al 6061 substrate appeared indented while, in others, it remained level or nearly level with respect to the overlying paint/binder layer. One observation consistent with all craters was that carbon was ubiquitous and heterogeneously distributed. LABE views directly into the central depression of the craters showed regions enriched in carbon (Fig. 4) spatially associated with fine-grained regions composed primarily of a mixture of paint/binder. Typically, particles composed of paint/binder were embedded within and/or lying upon the C-rich phase(s).
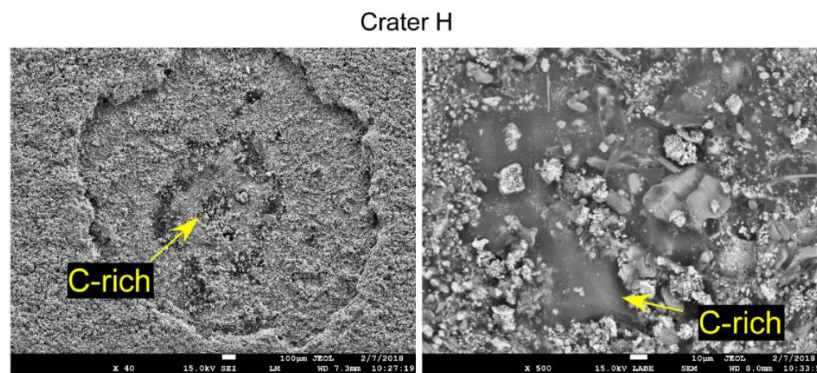

Fig. 4. FESEM/LABE images of Crater H. A low magnification (40X) image is shown at left with higher magnification (500X) image at the right. Locations of C-rich matter are noted for both. Visible in the left image is the entire spallation zone surrounding the central crater feature and the "walls" denoting the remnant paint layer.

In many of the craters, wispy, needle-like features composed of K and O were interspersed with the paint/binder. These features are interpreted as potassium hydrogen carbonate ($KHCO_3$) likely formed during exposure of WFPC-2 panel to the Florida coastal environment [1]. We note, however, that since they were coated with a layer of conductive carbon and were often spatially associated with epoxy, we could not determine the carbon content of this K-rich phase. To survey outcomes from the relatively simple to the complex, we will describe the analysis of craters H and M respectively. The analyzed cross-section of Crater M is shown in Fig. 5. This was an unusual crater in that it was composed of a single, shallow depression containing four layers, excluding epoxy. Proceeding from the outermost layers these were: (1) paint + other phases, (2) Al 6061, (3) Al 6061 with a high concentration of embedded particles, this layer was called the 'mid region,' and (4) Al 6061. In layers 2 and 4, embedded particles are present at significantly lower concentration than those in the 'mid region,' as clearly seen in both the LABE

view and the Al element map. The overview image of Crater M suggests a compound crater composed of multiple distinct, local depressions with a relatively flat geometry. Such craters are typical for aggregate particles in which dense components/minerals float in a friable and much less dense matrix. The detailed mass distribution of such an aggregate manifests itself in a compound crater morphology. If one accepts this interpretation, melts from neighboring depressions can overlap with each other to form layers 2 and 3—specifically layer 3 ('mid region') —a mixture of projectile and target-derived melts with Al being the dominant element. Interestingly, this outcome is consistent with internal hydrocode studies conducted in 2010. In this study, stainless steel (SS) projectile material was entrained in Kelvin-Helmholtz instabilities that form as the denser SS impacts the less dense Al target material. Particles located at the epoxy/layer 1 interface and within layer 3 in Crater M (Fig. 5) include brass (Cu/Zn), bismuth (Bi), Zn, and SS (Fe, Cr). The latter particle type (SS) displayed a composition different from that of the SS particles embedded within the Al 6061 matrix, as they did not contain detectable copper.
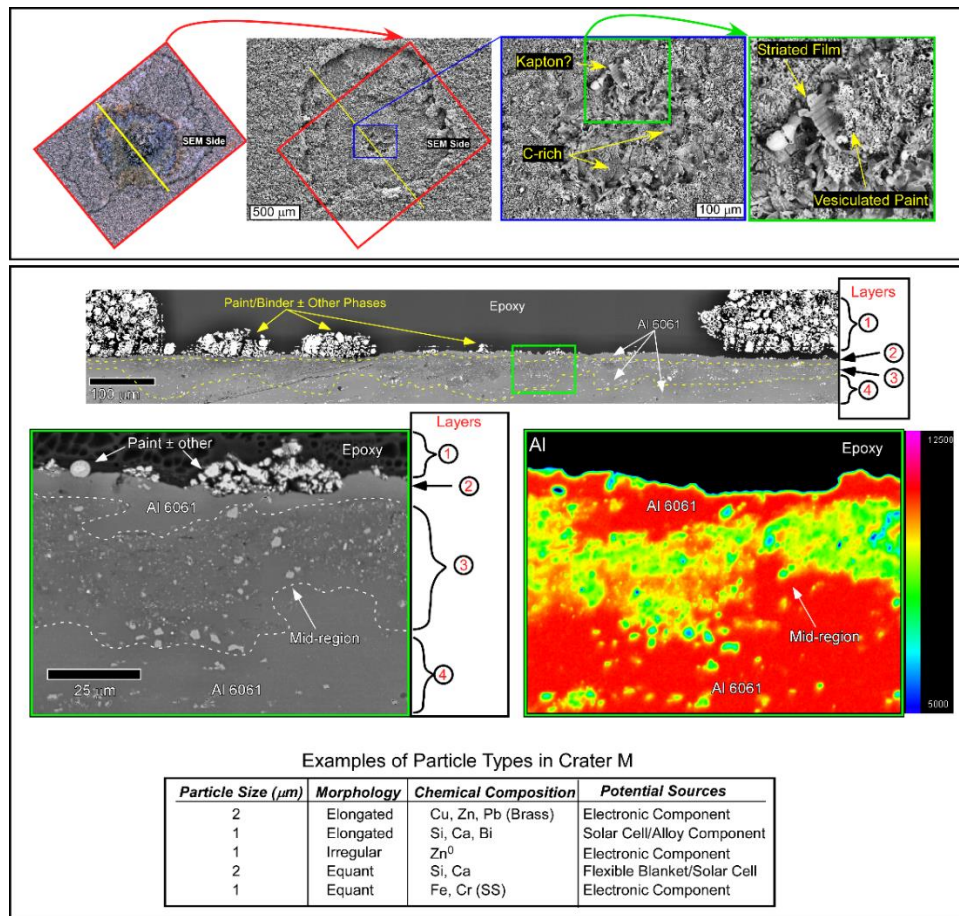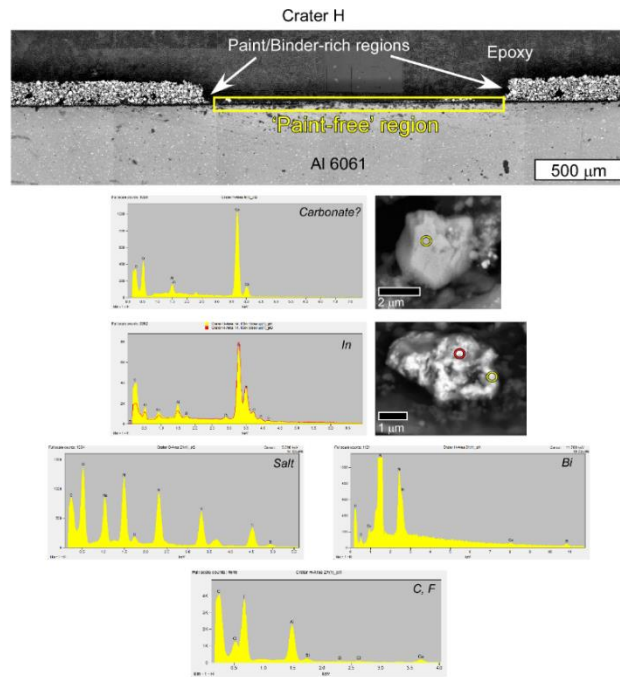

Examples of Particle Types in Crater M

Particle Size (μm)	Morphology	Chemical Composition	Potential Sources
2	Elongated	Cu, Zn, Pb (Brass)	Electronic Component
1	Elongated	Si, Ca, Bi	Solar Cell/Alloy Component
1	Irregular	Zn^0	Electronic Component
2	Equant	Si, Ca	Flexible Blanket/Solar Cell
1	Equant	Fe, Cr (SS)	Electronic Component

Fig. 5. Sample M imaged as a complete crater and after sectioning. ***Upper Box***, <u>*Left to right*</u>: Optical view of crater M with the Line of Interest/cut line in yellow. Location of the region outlined by the red box is shown in the FESEM/LABE view at right. Cut line (yellow) is also noted in this view. The region in the blue box is magnified at right and highlights the central crater depression. Locations of carbon-rich regions and a piece of film, possible Kapton, are noted. The region in the green box shows a magnified view of striated film with one edge embedded in vesiculated paint/binder. ***Lower Box***, *Top to Bottom:* FESEM/LABE image of a region of the polished section produced from crater M. Region in the green box is magnified in the lower left image. *Lower left*: High magnification of the region highlighted by the green rectangle in the upper view. An increase in particle density is seen in the 'Mid region' layer compared to layers 2 and 4. *Lower right*: EDX Al element map is shown for the region outlined by the green rectangle in the view at left. A decrease in Al concentration is seen in the 'mid-region' layer due to the increase in particle density. The table provides chemical composition and possible sources for particles associated with the crater M impactor.

Sample H was a simple crater with a relatively flat floor. The region designated as 'paint-free' contained several Ca-bearing, O-rich particles (see Fig. 6) with variable Ca:O ratios. None of the compositions approximated common Ca-rich mineral phases such as calcite ($CaCO_3$), portlandite ($Ca(OH)_2$) or lime (CaO). We suggest that the variety of Ca-bearing phases observed within Crater H is the result of the heterogeneous decarboxylation of $CaCO_3$ resulting from impact heating that produced residue with variable Ca:O ratios. This interpretation is supported by results from light-gas gun impact studies, performed at NASA/JSC in 2015 [14]. Analysis of the resultant impact craters showed mixing of impactor with the target producing residue within the craters composed of a mixture of Ca-bearing mineral phases ($CaCO_3$, $Ca(OH)_2$, CaO) intimately mixed with the Al substrate. Other particle compositions in Crater H are shown and include In, Bi, C, and fluorine (F), possibly polytetrafluoroethylene or Teflon, and likely terrestrial salts containing Na, K and S. Crater residue interpreted as being derived from MM impacts was not detected in Crater H. In summary, results indicate residues identified in craters listed in the table (Fig. 6) are consistent with terrestrial sources including satellite debris, natural phases (*e.g.*, minerals) and natural terrestrial contaminants (*e.g.*, salts, $KHCO_3$).

Examples of Particle Types in Crater H

Particle Size (μm)	Morphology	Chemical Composition	Potential Sources
4	Equant	C, Ca, O	Terrestrial/Natural
5	Irregular	In	Solar Cell
5	Irregular	C, F	Insulation (Polytetrafluoroethylene)
1	Irregular	Bi	Alloy
1	Irregular	Na, K, S	Terrestrial/Natural

Fig. 6. *Upper view*: Low magnification FESEM/LABE image of the center depression of the thin section of crater H. Particles characterized by EDX spectra are located in the 'Paint-free region.' *Lower views*: EDX spectra and FESEM/LABE images of particles located at the interface of the Al 6061 matrix and the epoxy. Particles are composed of possible carbonate (calcite), indium (In), salts (Na, S, and K), Bi, and C and F (polytetrafluoroethylene/Teflon).

8   DISCUSSION

The presence of distinct C-rich phases in every crater analyzed in this study is striking. The C-rich matter was recognizably different in nature from epoxy and partially coated the floor and/or lower sides of each crater. This matter contained major C and O and minor Na, S, and K, with embedded particulates of the thermal control paint. The carbon abundance that can be inferred for the impactors is too high to be consistent with a typical meteoritic (*i.e.*, chondritic) source; we suggest it resulted from impact debris produced from C-bearing composites and/or laminates used in spacecraft structural supports. These impacts may have resulted from a single source that

separated into multiple pieces or may have resulted from an aggregation, or cloud, of particles produced from primary, secondary, and even tertiary impact events. The lack of any particles embedded in the C-rich matter that could be interpreted as MM (*e.g*., silicates [olivine, pyroxene]) indicates that the material did not originate from extraterrestrial sources. Mineral grains comprising interplanetary dust particles/meteorites would typically have been detected in the craters, as shown by numerous other studies [15, 16. 17, 18, 19]. The second key observation is the presence of particles consistent with OD sources embedded in the paint/binder or located at the paint layer/Al 6061 interface. None of the particles analyzed were consistent with those that could be interpreted as MMs. OD element indicators include Ce and Mo from flexible blankets/solar cells, C and F from polytetrafluoroethylene, metals from electronic components (*e.g*., indium (In), Bi, Zn, Cu/Zn, lead (Pb), platinum (Pt), Sn, zirconium (Zr), Ni), minerals (*e.g*., calcite) from terrestrial sources, and several types of salts, likely terrestrial contaminants. Results to date have been examined in the context of validating the NASA ODPO OD engineering model in development, ORDEM 3.1 [20]. A comparison of WFPC-2 analysis results to date and the total MMOD flux are presented therein, with good agreement.

9   CONCLUSIONS

In this paper, we have briefly described the characterization of impact feature samples from the HST's WFPC-2 radiator using a new, partially destructive technique that reveals the crater/substrate interface. FESEM/EDX characterization of polished sections of large craters has revealed new information on the abundance and types of particles associated with the WFPC-2 radiator impactors. Despite potential limitations of the lateral surface inspection technique (while noting that a sample may be re-polished to reveal a new surface), the opinion of the analytical staff is that this analysis scheme provides a better approach to determining impactor type by removing certain physical and instrumental constraints. Large cores have been returned to NASA JSC from the Natural History Museum and will be processed in a similar manner to expand the dataset and our understanding of the low Earth orbit environment.

10   REFERENCES

1. Kearsley A.T., *et al*. Micrometeoroid Impacts on the Hubble Space Telescope Wide Field and Planetary Camera 2: Larger Particles. LPSC 45, #1722, 2014.

2. Ross D.K., *et al*. Micrometeoroid Impacts on the Hubble Space Telescope Wide Field and Planetary Camera 2: Smaller Particle Impacts. LPSC 45, #1514, 2014.

3. Anz-Meador, P. D., *et al*. "Sampling and Analysis of Impact Crater Residues Found on the Wide Field Planetary Camera-2 Radiator." Ed. L. Ouwehand. Sixth European Conference on Space Debris, Proceedings of the Conference (22-25 April 2013, in Darmstadt, Germany). ESA SP-723, 2013.

4. Graham, G.A., Kearsley, A.T., Drolshagen, G., *et al*. Micro-particles impacts upon HST solar cells. Adv. Space Res. 28, pp. 1341–1346, 2001.

5. Graham, G.A., McBride, N., Kearsley, A.T., *et al.* The chemistry of micrometeoroid and space debris remnants captured on Hubble Space Telescope solar cells. Int. J. Impact Eng. 26, pp. 263–274, 2001.

6. Kearsley A.T., et al. Impacts on Hubble Space Telescope solar arrays: discrimination between natural and manmade particles. Adv. Space Res. 35, pp. 1254-1262, 2005.

7. Kearsley A.T., *et al*. Hypervelocity impact in low earth orbit: Finding subtle impactor signatures on the Hubble Space telescope. 14th Hypervelocity Impact Symposium 2017, HVIS2017, April 24-28 2017, Canterbury, Kent UK, Procedia Engineering 204, pp. 492-499, 2017.

8. Opiela J.N., Liou J.C., Anz-Meador P.D. Micrometeoroid and Orbital Debris Impact Feature Size and Position Data Collected During the Post Flight Survey of the Hubble Wide Field Planetary Camera 2. NASA/TP2012217359, 2012.

9. Bernhard, R.P., *et al*., "Composition and Frequency of Impact residues Detected on LDEF Surfaces." Proc. First European Conf. Space Debris ESA-SD-01 (July 1993), pp. 189-94, 1993.

10. Grün, E., *et al*., "Collisional Balance of the Meteoritic Complex" Icarus 62, pp. 244-72, 1985.

11. Wozniakiewicz, P., *et al*. In situ analysis of residues resulting from laboratory impacts into aluminum 1100 foil: Implications for Stardust crater analyses. Meteoritics and Planetary Science 44, pp. 1541-1559, 2009.

12. Ferrari A. C. and Robertson J. Interpretation of Raman spectra of disordered and amorphous carbon. *Physical Review B* 61, pp. 14095 – 14107, 2000.

13. Robertson J. Diamond-like amorphous carbon. *Materials Science and Engineering* R37, pp. 129–281, 2002.

14. Hörz, F., *et al*. Unconfined impact experiments: A pilot study in to the shock induced melting and devolatilization of calcite. Submitted to Meteoritics and Planetary Science, 2019.

15. Zolensky M.E., et al. Simon C.G. & Kinard, W.H., Interim report of the meteoroid debris special investigation group, *Proc. Second LDEF Post-Retrieval Symp.* NASA CP-3194, 1993**.**

16. Zolensky M.E., See T.H., Bernhard R.P., *et al*. Final activities and results of the Long Duration Exposure Facility meteoroid and debris special investigation group. *Adv. Space Res*. 16, (11)53-(11)65, 1995.

17. Graham G.A., Sexton A., Grady M.M., Wright I.P. Further attempts to constrain the nature of the impact residues in the HST solar array panels. Adv. Space Res. 20, pp. 1461-1465, 1997.

18. Graham G.A., *et al*. Hypervelocity impacts in low Earth orbit: Cosmic dust versus space debris. Adv. Space Res. 23, pp. 95-100, 1999.

19. Yano H., et al. Origins of micro-craters on the SFU spacecraft derived from elemental and morphological analyses. *Adv. Space Res*. **25**, pp. 293-298, 2000.

20. Matney, M., P. Manis, P. Anz-Meador, D. Gates, J. Seago, A. Vavrin, and Y.-L. Xu. "The NASA Orbital Debris Engineering Model 3.1: Development, Verification, and Validation," Paper presented at the 1st International Orbital Debris Conference, Sugar Land, TX, 9-12 December, 2019.